Radiation hardness of three-dimensional polycrystalline diamond detectors

Stefano Lagomarsino,[1,2,a)] Marco Bellini,[3,4] Chiara Corsi,[2,3] Vladimir Cindro,[5] Keida Kanxheri,[6,7] Arianna Morozzi,[8] Daniele Passeri,[6,8] Leonello Servoli,[6,7] Christian J. Schmidt,[9] and Silvio Sciortino[1,2]

[1] *National Institute of Nuclear Physics (INFN), Via B. Rossi, 1-3, 50019 Sesto Fiorentino (FI), Italy*

[2] *Department of Physics and Astronomy, University of Florence, Via G. Sansone 1, 50019 Sesto Fiorentino (FI), Italy*

[3] *European Laboratory for Non-Linear Spectroscopy, Via Nello Carrara 1, 50019 Sesto Fiorentino (FI), Italy*

[4] *Istituto Nazionale di Ottica (INO-CNR), Largo Enrico Fermi 6, 50125 Firenze (FI), Italy*

[5] *Jozef Stefan Institute, Jamova cesta 39, 1000 Ljubljana, Slovenia*

[6] *National Institute of Nuclear Physics (INFN), Via A. Pascoli, 06123 Perugia (PG), Italy*

[7]

[8] *Department of Engineering, University of Perugia, Via G. Duranti 93, 06125 Perugia (PG), Italy*

[9] *GSI Helmholtzzentrum für Schwerionenforschung, Planckstraße 1, 64291 Darmstadt, Germany*

The three-dimensional concept in particle detection is based on the fabrication of columnar electrodes perpendicular to the surface of a solid state radiation sensor. It permits to improve the radiation resistance characteristics of a material by lowering the necessary bias voltage and shortening the charge carrier path inside the material. If applied to a long-recognized exceptionally radiation-hard material like diamond, this concept promises to pave the way to the realization of detectors of unprecedented performances. We fabricated conventional and three-dimensional polycrystalline diamond detectors, and tested them before and after neutron damage up to $1.2 \times 10^{16}\,\mathrm{cm}^{-2}$, 1 MeV-equivalent neutron fluence. We found that the signal collected by the three-dimensional detectors is up to three times higher than that of the conventional planar ones, at the highest neutron damage ever experimented.

Resistance to radiation damage is one of the main challenges in the development of detector systems located in the vicinity of the beam interaction zones, in upcoming high luminosity high energy physics experiments.[1] Radiation damage is due to the formation of point and cluster defects generated by nuclei displacement inside the lattice, the latter produced if the primary knock-on atom has an energy sufficient to trigger a cascade. Such defects degrade the performances of solid state detectors in term of collected charge, response time, working temperature, and bias-voltage, up to a level dependent on the integrated fluence of energetic particles, which is expected to increase of at least a factor ten in the experiments planned in the next future.[2]

Diamond, as an active material in solid state detectors, offers a combination of exceptional properties which make it highly competitive in radiation-harsh environments. Its large band gap and large displacement energy make it a material inherently radiation tolerant with very low leakage currents, which can be operated without cooling.[3] Tiny leakage currents and small pixel capacitances, due to a lower dielectric constant of diamond with respect to silicon, result in low-noise performance of the associated front-end electronics.[4] Its large charge carrier saturation velocity and high mobility for both carriers,[5] combined with a large breakdown field, result in timing properties superior to all other known solid-state detectors.[6,7]

Recently, the three-dimensional (3D) concept has been implemented in diamond detectors, by pulsed laser fabrication of columnar electrodes perpendicular to the sensor surface, in order to shorten the inter-electrode distance without decreasing the overall charge generated in the material.[8–10] As a result, further advantages emerged: single-crystal 3D detectors reached a 95% collection efficiency at a bias voltage as low as 3 V.[8] Moreover, simulations of the behavior of this kind of detectors after heavy irradiation predict an increase of the signal level up to a factor 3, if compared to conventional planar diamond detectors.[11]

The main drawbacks of single-crystal diamond for tracking purposes are its present price and the small area of the available samples (at most about $8 \times 8\,\mathrm{mm}^2$), but polycrystalline diamond wafers grown in microwave chemical vapor deposition chambers can reach a size of about 120 mm diameter, comparable with that of the silicon wafers, and their cost per unit area is lower than that of the single-crystals by a factor three.[12] These are the reasons why a thorough investigation on the performances of polycrystalline three-dimensional diamond detectors under high radiation fluence is highly desirable.

We have fabricated three-dimensional radiation sensors in polycrystalline electronic-grade diamond plates, writing graphitic electrodes in the diamond bulk by means of pulsed laser irradiation. Then, we tested them for collection efficiency under ^{90}Sr-beta irradiation. We have compared their performances with those of conventional planar (2D) sensors fabricated on the same samples, before and after fast neutron irradiation up to a fluence of 1.2×10^{16} 1 MeV-equivalent

[a)]Author to whom correspondence should be addressed. Electronic mail: lagomarsino@fi.infn.it

neutrons per cm^2. As a result, we found that the average signals from the 3D detectors, for the highly damaged sensors, are about three times higher than those of the planar sensors.

We have also simulated the charge collection processes of the sensors by means of a 3D Monte Carlo method, and compared the experimental data with the charge collection efficiency predicted by a simple model of the generation of defects limiting the charge carrier lifetime in the diamond bulk. We have found that a simple model of the trapping mechanisms in the polycrystalline material gives account of both the 3D- and the 2D-sensors collection efficiency.

Twelve different sensors were fabricated on four polycrystalline $5 \times 5 \times 0.5\,mm^3$ diamond samples coming from a batch obtained by the same wafer of high quality electronic grade material.[13] The buried electrodes were written in the bulk diamond by means of a 800 nm Ti-sapphire laser source, with a 30 fs pulse width, about 6 μJ of energy per pulse and a repetition rate of 1 kHz, which causes a phase transition to a mixed sp^2-sp^3 carbon phase whose resistivity amounts to about 1 Ωcm.[14] The electrodes are stacked according to a two-dimensional grid with different pitches, whose "elementary cells" measure $100 \times 160\,\mu m^2$ ($3D_{100\times160}$ sensors) or $70 \times 114\,\mu m^2$ ($3D_{70\times114}$ sensors) (see Fig. 1). The electrodes were connected by means of superficial conductive combs engraved on the two sample surfaces by means of a different laser technique, employing 8 ns-long, 40 μJ-energy pulses from a 1 kHz Nd:YAG laser source.[15] The superficial conductive paths exhibit a resistivity of the order of some mΩcm (Ref. 14) and have a width of about 9 μm and a depth of about 7 μm. Each column has been started from a tooth of a superficial comb and ended at about 80 μm from the opposite surface, in order to avoid superficial currents. Conventional planar sensors were also fabricated as references, by writing opposite-sided superficial conductive combs with a pitch of 80 μm. All the fabricated sensors have a surface of about $1.5 \times 1.5\,mm^2$, in a way that 3 different sensors on a same sample could be arranged and connected to the readout electronics, one of each type (respectively, 2D, $3D_{100x160}$, and $3D_{70x114}$ sensors). A picture of one of the four samples with the integrated 3D and 2D sensors is shown in Fig. 1.

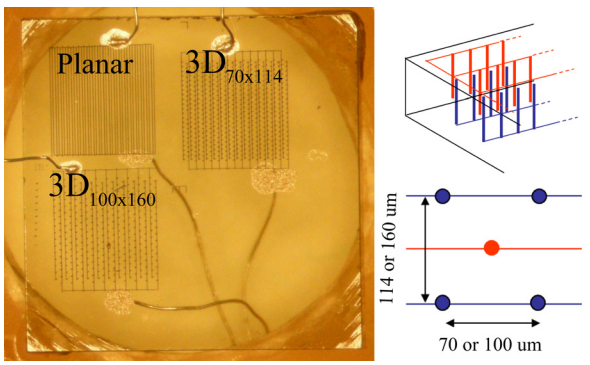

FIG. 1. One of the four samples under investigation with the three sensors and the silver-paste contacts connecting to the external electronics. At the right, schematics of the two opposite polarized arrays of columns, in blue and red. Each array starts from a graphitized comb on one side of the sample, the two arrays are staked in a way that the electric field has a bi-dimensional periodicity. At the bottom right, a sketch of an "elementary cell" of the structure with sense (red) and bias (blue) columns.

We irradiated the four diamond samples at the experimental nuclear reactor of the Jozef Stefan Institute of Ljubljana (SLO), with fast neutron (neutrons of energy greater than 100 keV) at fluences ranging from $2.2 \times 10^{14}\,cm^{-2}$ to $10^{16}\,cm^{-2}$. The hardness factor of the neutron spectra has been evaluated considering the non-ionizing energy loss (NIEL) of neutrons in the range of 100 keV−30 MeV, normalized to the NIEL of neutrons at 1 MeV.[16] The resulting fluences, in 1 MeV-equivalent neutrons, were 2.64×10^{14}, 3×10^{15}, 6×10^{15}, and $1.2 \times 10^{16}\,cm^{-2}$.

After neutron irradiation, we have also fabricated, on the sample irradiated at $3 \times 10^{15}\,cm^{-2}$ 1 MeV-equivalent neutrons, a new 2D sensor of the same size, writing superficial combs interdigitated with the old ones, and a new $3D_{70\times114}$ sensor on the sector of the sample left free by the other detectors. This new sensors were fabricated in order to verify if neutron irradiation degrades the performances of the graphitic contacts.

The charge collection efficiencies of all the sensors were tested before and after the neutron damage, under irradiation with ^{90}Sr-beta electrons. For the electrons having an energy sufficient to pass through the diamond and trigger the measurement, the average number of electron-hole pairs generated in the bulk diamond does not differ more than about 8% from the value obtained by a charged particle at minimum ionizing energy.[17] The measurement chain[18] consists of a scintillator plastic placed under the sensor under test, providing the trigger signal, an Amptek A250 integrating stage buffered by an input FET, an Amptek A275 formation stage, and a 12 digit analog-to-digital converter sampling the shaped signal at 1.4 μs from the trigger. The collected charge is derived by the maximum output voltage of the shaper with a calibration constant evaluated in 220 elementary charges/mV with a 15%, uncertainty. The measurement noise, in elementary charges, amounts to about 300. This permits, with the reasonable statistics of some tens of thousands events, the relative comparison of the charge collection efficiencies of the sensors with a percent accuracy. In order to collect signals in stable conditions, each sample has been primed by beta irradiation to fill the native or damage-induced deep traps in the material[19] and to reach the limit value of the carrier lifetime. The necessary priming dose has been found to be very different for unirradiated and irradiated samples: 5 Gy are sufficient in the former case, while about 100 Gy are necessary in the latter.

The charge collection was measured before neutron irradiation at several bias voltages, and the results are shown in Fig. 2.

The saturation collected charge of the three type of sensors was evaluated by means of a simple Hecht fit[20] as 8700 ± 300, 7200 ± 300, and 7100 ± 200 elementary charges for the $3D_{70x114}$, the $3D_{100x160}$, and the 2D sensor, respectively. The 90% of these values were reached at a bias voltage of 45 V, 60 V, and 450 V, respectively. It is then confirmed that signal saturation occurs at a bias level about one order of magnitude lower for the 3D than for the 2D sensors, also for polycrystalline detectors as for the monocrystalline ones. Noticeably, the upper limit signal of the $3D_{100x160}$ and that of the 2D sensor have about the same value, but the

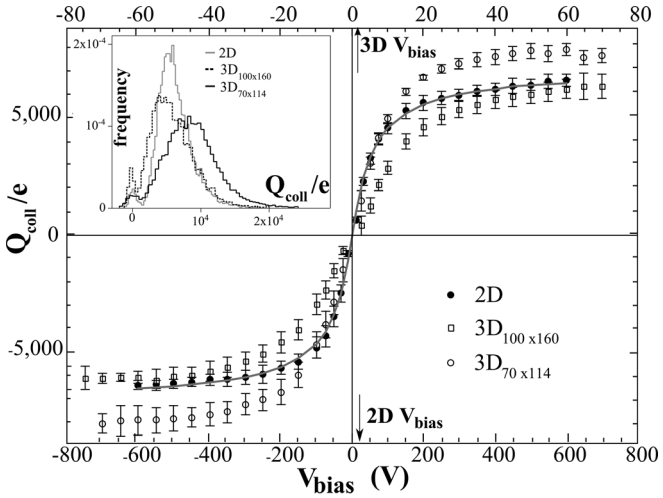

FIG. 2. The dependence of the average charge signal on the bias voltage for the 3D and for the planar sensors. The average is performed over the values given by four sensors of the same type, and the error bar is referred to the standard deviation from the average. Note the different bias voltage scale employed for the planar and for the 3D sensors. The continuous line represents the fit of the planar sensors collected charge obtained by the Hecht formula (Eq. (1)). In the inset, the signal distribution, at saturation, for each sensors type.

$3D_{70\times114}$ sensors yield a collection efficiency about 20% higher.

A clear understanding of the behavior of these detectors requires an analysis taking into account the polycrystalline structure of the material.

Grain boundaries are extended regions with a high density of trapping impurities. While the trapping probability of a charge carrier in the bulk regions during a small time dt can be assumed to equal the ratio dt/τ (τ being the trapping time, assumed equal for electrons and holes), charge carriers are expected to be trapped at the grain boundaries only when their path crosses the surface delimiting two neighbor grains. Consequently, the trapping probability at grain boundaries along a small path of length ds is more properly evaluated as ds/λ_g, where λ_g is a mean free path limited by the grain boundaries only. The overall trapping probability during a path of length ds can thus be given by $\frac{ds}{\lambda}$, with $\frac{1}{\lambda}=\frac{1}{\lambda_g}+\frac{1}{v_d(E)\tau}$, where λ is the overall mean free path, v_d is the drift velocity, dependent on the electric field, while λ_g is bias-independent.

Assuming $v_d(E)=\frac{\mu E}{1+\mu E/v_{sat}}$ ($\mu=$ carrier mobility $\approx 2\times10^3$ cm^2/(V s), and $v_{sat}=$ saturation velocity $\approx 2\times10^7$ cm/s), and using the well-known Hecht formula[20] for the charge collection efficiency (CCE, ratio of the collected to the generated charge)

$$CCE=2\left[\frac{\lambda}{L}-\frac{\lambda^2}{L^2}\left(1-e^{\frac{-L}{\lambda}}\right)\right] \qquad (1)$$

($L=$ sensor thickness), we can fit the experimental points for the CCE of the planar sensors, obtaining a very good fit with $\tau=4.3$ ns and $\lambda_g=160\,\mu$m (see Figure 2).

The behavior of the 3D sensor differs from that of the planar one in an important respect. While the trapping probability in the bulk of the grains can be expected to be equal for the two configurations, the conic-columnar shape of the grains, typically extending from one face to the other of the diamond sample, implies a very different grain boundaries-limited mean free-path λ_g for the 2D and for the 3D sensors, due to the different path of the carriers in the two structures.

We have simulated the CCE of both the 3D sensors at saturation, by means of an algorithm taking into account the full three-dimensional finite element calculation of the electric field with a commercial TCAD tool,[21] and a Monte Carlo simulation of the charge generation, performed in random points of the diamond bulk (see Fig. 3). We adjusted the grain boundary-limited mean free path λ_g to fit to the CCE at saturation of the $3D_{100\times160}$ and of the $3D_{70\times114}$ sensors, assuming as a constant the bulk trapping time $\tau=4.3$ ns (as in the 2D configuration). We found very similar values for λ_g, respectively, 29 and 25 μm (to be compared with 160 μm with the 2D sensors). The reason why, notwithstanding a much shorter λ_g, we obtain comparable efficiencies for the 3D and the 2D sensors, is of course the lower trapping probability due to the much shorter effective path of the carriers in the 3D sensors, determining a slightly higher CCE for the sensors with the closer electrodes. As we shall see in brief, this fact is also at the origin of the much better behavior of the 3D sensors after neutron damage.

The collection efficiency of each sensor has also been measured after irradiation for all the samples under test, and the results are summarized in Figure 4.

The results from the planar sensors allow the immediate evaluation of the *hardness factor* K of the material, defined by the following relation:

$$\frac{1}{CCE}=\frac{1}{CCE_0}+LK\phi. \qquad (2)$$

In Eq. (2), CCE and CCE_0 are the collection efficiencies in the damaged and in the undamaged state, respectively, at the saturation bias field of 1 V/μm; ϕ is the radiation fluence; L is the detector thickness, and K depends on the radiation species and energy. Equation (2) is usually expressed, in literature, in term of a "charge collection distance" $CCD\equiv L\times CCE$, giving a measure of the mean length a hole and an electron drift apart before trapping. The value of the hardness factor K deduced by fitting our measurements of the planar sensors

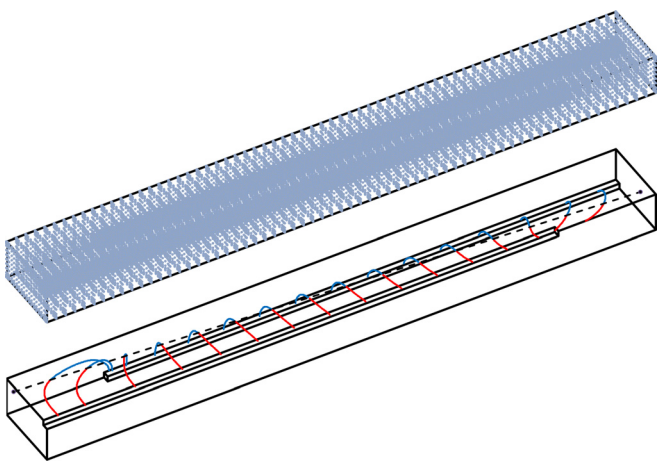

FIG. 3. Schematics of one of the 3D simulation cells (for the 70 $\times$ 114 μm^2 geometry). Above: The simulation grid employed to calculate the electric field. Below: some of the possible trajectories of the charges generated along the path of an ionizing particle.

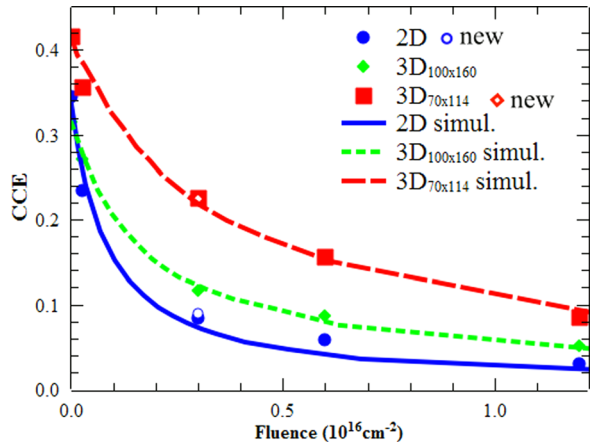

FIG. 4. CCE measured with each type of sensor as a function of the radiation damage suffered. Dots: Measured values with the 3D and 2D sensors after neutron damage, as a function of the neutron fluence. Empty dots: CCE of the sensors fabricated after damage (new). Lines: simulation of the charge collection efficiency of each kind of sensor as a function of the neutron fluence.

efficiency is $(4.7 \pm 0.2) \times 10^{-18}\,\mu\text{m}^{-1}\,\text{cm}^2$, which is compatible with the most accurate previously reported[22] value of $(4.2 \pm 0.8) \times 10^{-18}\,\mu\text{m}^{-1}\,\text{cm}^2$.

The most important feature emerging from the measurements is that the 3D efficiencies, despite their values are about the same of the 2D sensors at low fluences, gain a factor 3 beyond $3 \times 10^{15}\,\text{cm}^{-2}$ of 1 MeV-neutron fluence. It is also of interest that the sensors fabricated before and after irradiation, in the same sample irradiated at 3×10^{15} neutrons/cm^{-2}, exhibit signals which, after damage, are not significantly different. This fact clearly indicates that graphite-diamond contacts are not affected by radiation damage.

The factor 3 in efficiency gained by the irradiated 3D detectors with the smaller pitch can be accounted for assuming that neutron damage results in the introduction of new inter-bandgap levels reducing the bulk mean-life time of the charge carriers, leaving unaffected the grain boundaries-limited mean free path λ_g.

For not too high fluences, the density of the induced defects can be assumed to be proportional to the fluence ϕ, in a way that the mean path-length λ of the charge carriers can be written as

$$\frac{1}{\lambda} = \frac{1}{\lambda_g} + \frac{1}{v_d(E)}\left(\frac{1}{\tau} + k\phi\right), \tag{3}$$

where the constant k, proportional to the cross section for the production of a trapping defect by neutron irradiation, depends both on the type and the energy of the damaging particles. The constant k is correlated but not merely proportional to the hardness factor K, inasmuch the *CCE* of a planar detector in Eq. (2) is only roughly proportional to λ/L, according to Eq. (1).

We have calculated the collection efficiency of the 2D and 3D sensors for different values of the product $k\phi$, keeping the values of λ_g and τ equal to those found for the undamaged samples. The efficiency of the 2D detectors was calculated by means of the Hecht formula, while for the 3D sensors the same Monte Carlo simulation of the charge collection of the 3D structures has been employed, as done for the CCE before damage. Then, we varied the constant k in a way to fit the calculated values of the CCE to the measured ones as functions of ϕ.

We found that the damage curves of all the sensors are fitted by very close values of the constant k (see Figure 4), namely, 1.46×10^{-6}, 1.57×10^{-6}, and $1.63 \times 10^{-6}\text{cm}^2$ Hz, respectively, for the 2D sensors, for the $3D_{100\times160}$ and for the $3D_{70\times114}$. The independence of the factor k on the electrodes configuration confirms that Eq. (3) gives account of the behavior of charge carriers in the material, both regarding to the separation of the trapping probability in two contributions (bulk and grain boundary) and to the dependence of the bulk trapping on the radiation damage.

We observe that the better behavior of the 3D sensors, after damage, can be explained noting that the term $\frac{k\phi}{v_d}$ in Eq. (3), which is the same for the 2D and the 3D sensors, has a smaller relative weight for the 3D sensors if compared with the inverse of the grain boundaries-limited mean free path $\frac{1}{\lambda_g}$.

Consequently, once the effect of a smaller λ_g is compensated by making the electrodes closer to each other, the weight of the defects induced by radiation damage is correspondingly lower.

In conclusion, we have proved that three-dimensional diamond sensors are able to collect measurable single event signals after a level of radiation damage which makes unusable conventional planar diamond sensors, whose exceptional radiation hardness has been studied and recognized for long. As a consequence, it is fair to assume that in the next future this kind of detector may well become a reference for resistance in radiation harsh environments.

This research was funded by the European Union (HadronPhysics3 Project No. 283286), the GSI (Darmstadt) within the frame of the "Detector technology and systems platform" of the Helmoltz association, and the National Institute of Nuclear Physics (INFN), Italy, in the frame of the experiment 3D_SOD. We would like to thank Mirko Brianzi of INFN and Vincenzo Greco, Mauro Pucci, Andrea Sordini of INO-CNR (Florence) for their invaluable technical support in the preparation and characterization of the diamond samples.

[1]E. Berdermann, M. Pomorski, W. de Boer, M. Ciobanu, S. Dunst, C. Grah, M. Kiš, W. Koenig, W. Lange, W. Lohmann, R. Lovrinčić, P. Moritz, J. Morse, S. Mueller, A. Pucci, M. Schreck, S. Rahman, and M. Träger, "Diamond detectors for hadron physics research," Diamond Relat. Mater. **19**(5–6), 358–367 (2010).

[2]F. Gianotti, M. L. Mangano, T. Virdee, S. Abdullin, G. Azuelos, A. Ball, D. Barberis, A. Belyaev, P. Bloch, M. Bosman *et al.*, "Physics potential and experimental challenges of the LHC luminosity upgrade," Eur. Phys. J. C **39**, 293–333 (2005).

[3]H. Kagan and W. Trischuk, *Radiation Sensors for High Energy Physics Experiments, in CVD Diamond for Electronic Devices and Sensors* (Wiley, 2009).

[4]J.-W. Tsung, M. Havranek, F. Hügging, H. Kagan, H. Krüger, and N. Wermes, "Signal and noise of diamond pixel detectors at high radiation fluences," JINST **7**, P09009 (2012).

[5]J. Isberg, J. Hammersberg, E. Johansson, T. Wikström, D. J. Twitchen, A. J. Whitehead, S. E. Coe, and G. A. Scarsbrook, "High carrier mobility in single-crystal plasma-deposited diamond," Science **297**(5587), 1670–1672 (2002).

[6]M. Pomorski, E. Berdermann, A. Caragheorgheopol, M. Ciobanu, M. Kiš, A. Martemiyanov, C. Nebel, and P. Moritz for the NoRHDia Collaboration, "Development of single-crystal CVD-diamond detectors for spectroscopy and timing," Phys. Status Solidi A **203**(12), 3152 (2006).
[7]M. Ciobanu, E. Berdermann, N. Herrmann, K. D. Hildenbrand, M. Kiš, W. Koenig, J. Pietraszko, M. Pomorski, M. Rebisz-Pomorska, and A. Schüttauf, "In-beam diamond start detectors," IEEE Trans. Nucl. Sci. **58**(4), 2073 (2011).
[8]S. Lagomarsino, M. Bellini, C. Corsi, F. Gorelli, G. Parrini, M. Santoro, and S. Sciortino, "Three-dimensional diamond detectors: Charge collection efficiency of graphitic electrodes," Appl. Phys. Lett. **103**, 233507 (2013).
[9]A. Oh, B. Caylar, M. Pomorski, and T. Wengler, "A novel detector with graphitic electrodes in CVD diamond," Diamond Relat. Mater. **38**, 9 (2013).
[10]B. Caylar, M. Pomorski, and P. Bergonzo, "Laser-processed three dimensional graphitic electrodes for diamond radiation detectors," Appl. Phys. Lett. **103**, 043504 (2013).
[11]S. Lagomarsino, G. Parrini, S. Sciortino, M. Bellini, C. Corsi, F. Gorelli, and M. Santoro, "Pulsed laser fabrication of 3D diamond detectors," in Proceedings of the 11th International Conference on Large Scale Applications and Radiation Hardness of Semiconductor Detectors, PoS(RD13)010.
[12]See http://www.e6cvd.com/cvd/page.jsp?pageid=415 for a price list of standard dimensions diamond plates.
[13]See http://www.e6.com/wps/wcm/connect/E6_Content_EN/Home for the website of the manufacturer.
[14]S. Lagomarsino, M. Bellini, C. Corsi, S. Fanetti, F. Gorelli, I. Liontos, G. Parrini, M. Santoro, and S. Sciortino, "Electrical and Raman-imaging characterization of laser-made electrodes for 3D diamond detectors," Diamond Relat. Mater. **43**, 23 (2014).
[15]G. Parrini, F. Fabbrizzi, S. Lagomarsino, L. Nunziati, S. Sciortino, and A. Scorzoni, "Laser graphitization for polarization of diamond sensors," in Proceedings of 10th International Conference on Large Scale Applications and Radiation Hardness of Semiconductor Detectors, PoS(RD11)017, Firenze, Italy, 6–8 July 2011.
[16]R. S. Caswell, J. J. Coyne, and M. L. Randolph, "Kerma factors for neutron energies below 30 MeV," Radiat. Res. **83**, 217–254 (1980).
[17]S. Zhao, "Characterization of the electrical properties of polycrystalline diamond films," Dissertation (The Ohio State University, 1994).
[18]S. Sciortino, S. Lagomarsino, and F. Nava, "Silicon carbide for high signal to noise ratio MIPs detection from room temperature to 80 C," IEEE Trans Nucl. Sci. **56**(4), 2538 (2009).
[19]E. Borchi, S. Lagomarsino, S. Mersi, and S. Sciortino, "Model of carrier dynamics in chemical vapor deposition diamond detectors," Phys. Rev. B **71**, 104103 (2005).
[20]K. Hecht, "Zum Mechanismus des lichtelektrischen Primärstromes in isolierenden Kristallen," Z. Phys. **77**(3–4), 235–245 (1932).
[21]Synopsys SENTAURUS TCAD I-2013.12, see http://www.synopsys.com.
[22]G. Kramberger, "Radiation damage in diamond detectors," Vertex 2012—the 21st International Workshop on Vertex Detectors, 17–21 September 2012, Seogwipo, South Korea. See http://indico.cern.ch/event/190941/session/4/contribution/13/material/slides/0.pdf.